Frontiers of Information Technology & Electronic Engineering
www.jzus.zju.edu.cn; engineering.cae.cn; www.springerlink.com
ISSN 2095-9184 (print); ISSN 2095-9230 (online)
E-mail: jzus@zju.edu.cn

A microstrip filter direct-coupled amplifier based on active coupling matrix synthesis*

Yang GAO†1, Fan ZHANG[2], Yingying QIAO[1], Jiawei ZANG[3], Lei LI†‡1, Xiaobang SHANG[4]

[1]*School of Physics and Microelectronics, Zhengzhou University, Zhengzhou 450001, China*

[2]*School of Physics, University of Electronic Science and Technology of China, Chengdu 610054, China*

[3]*CTTL-System Laboratory, China Academy of Information and Communications Technology, Beijing 100191, China*

[4]*National Physical Laboratory, Teddington TW11 0LW, UK*

†E-mail: gaoyang678@outlook.com; lilei@zzu.edu.cn

Received June 16, 2020; Revision accepted Mar. 24, 2021; Crosschecked Aug. 31, 2021

Abstract: This paper presents a methodology of designing an amplifier integrated with a microstrip filter using an active coupling matrix. The microstrip filter is directly coupled to the active device, and the integrated filter amplifier can achieve filtering as well as matching functionalities, simultaneously, eliminating the need for separate matching networks. The filter amplifier is represented by an active coupling matrix, with additional columns and rows in the matrix corresponding to the active transistor. The matrix can be used to calculate the S-parameter responses (i.e., the return loss and the gain) and the initial dimensions of the integrated device. Moreover, the integration of a filter and an amplifier leads to a reduced loss and a more compact architecture of the devices. An X-band microstrip filter amplifier has been designed and demonstrated as an example. Microstrip technology has been chosen because of its appealing advantages of easy fabrication, low cost, and most importantly, easy integration with active devices.

Key words: Amplifier; Filter–amplifier integration; Microstrip; Coupling matrix
https://doi.org/10.1631/FITEE.2000292 **CLC number:** TN454

1 Introduction

Amplifiers are essential components in electronic systems, and are usually designed according to the specifications related to the requirements for electrical, thermal, and physical performance, and the cost (Gonzalez, 1996; Schwierz and Liou, 2002; Bahl, 2008). In microwave systems, amplifiers are usually connected to filters which are employed to select the desired frequency bands. They are commonly designed separately matching a 50-Ω impedance and then are cascaded in the system. Matching circuits are usually required to convert the complex impedance value of the transistor to 50 Ω. For the amplifier described in this paper, the separate matching structures have been removed. Instead, the amplifier is directly coupled to resonator-based filters, and this approach can reduce additional losses (due to matching structures) and increase the integration (due to the reduced overall size of components). A generic example of the filter and amplifier in a system is shown in Fig. 1; this is a receiver. Compared with the conventional amplifier connecting filter topology, the integrated filter amplifier replaces the input matching network (IMN) within the amplifier with the resonator-based filter.

Amplifier design technologies and fabrication processes generally depend on their categories and applications. Circuit types including metallic waveguide, coaxial waveguide, cavities, planar structure,

‡ Corresponding author

* Project supported by the National Natural Science Foundation of China (No. 62001520)

ORCID: Yang GAO, https://orcid.org/0000-0002-3282-1618; Fan ZHANG, https://orcid.org/0000-0001-6500-1598; Lei LI, https://orcid.org/0000-0001-7394-4094

or a hybrid form of those different geometries can be used. For low-noise amplifiers, the maximum power gain and the optimal noise figure are balanced goals, and usually, a compromise can be reached depending on certain conditions (Pozar, 2012). Typical examples of matching networks are those formed of structures such as stubs, quarter-wavelength transformers, and coupled lines. Most traditional matching technologies are based on microwave circuit analysis. For examples, single co-planar waveguide (CPW) line stubs were applied as the matching network (Kumar et al., 2017); step ridges behaved as the matching structure for the on-chip transistor in the Ku-band low-noise amplifier (LNA) (Courtney et al., 2015); antipodal fin-line arrays were employed in a coaxial waveguide for a GaAs monolithic microwave integrated circuit (MMIC) (Aljarosha et al., 2017). The matching circuits provide filter matching circuits for transistor devices (Chang and Itoh, 1990; Chun et al., 2002; Ito et al., 2004; Darcel et al., 2005; Lin et al., 2013). The similarity of the design methodologies (Chun et al, 2002; Lin et al., 2013) lies in the fact that the matching networks are modelled based on their equivalent circuit. However, transitions between the independent components bring extra losses and increase the circuit complexity. For the filter direct-coupled amplifier design approach (Chun et al., 2005; Chen et al., 2013a, 2013b; Gao et al., 2018), planar circuit elements are eliminated through a resonator-based filter, resulting in a reduced loss. The novelty also lies in the design methodology; the physical matching structure can be determined directly through the coupling strength instead of modeling the matching circuits. This enhances the amplifier design efficiency.

The active coupling matrix of filter direct-coupled amplifiers was proposed in Gao et al. (2018), in which additional rows and columns were introduced denoting the transistor. Then, an N+4 coupling matrix was developed for active device coupling in the middle of the resonators (Gao et al., 2019, 2020). The novel active coupling matrices were employed to facilitate the filter structure, in which physical dimensions were determined by the internal and external coupling coefficients. This paper will present the detailed process of the matrix manipulation, including normalization using cofactor and determinant formulas. This has not been previously considered in Gao et al. (2018, 2019, 2020). This is also the first time that a microstrip filter amplifier has been implemented using active coupling matrix synthesis. Compared with waveguide-based devices, microstrip technology has advantages of lower manufacturing cost, easier fabrication, and most importantly, easier integration with on-chip active devices. Microstrip is also the most common choice in general microwave applications, and therefore the design of a filter amplifier described here could be of great interest.

The matrix scaling process is presented in detail to illustrate the active matrix normalization. An X-band microstrip filter amplifier is demonstrated as an example, showing the procedure for extraction of dimensions and design of filter direct-coupled amplifiers.

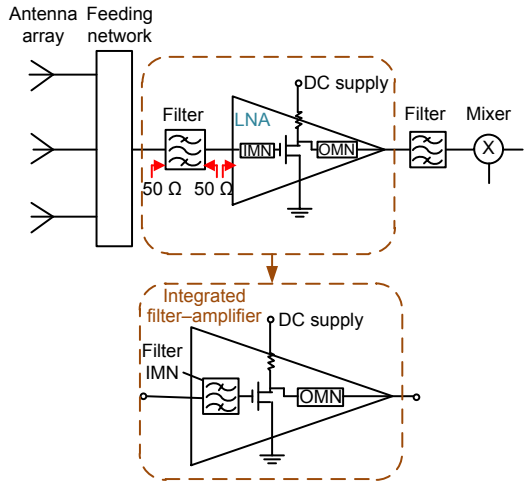

Fig. 1 Conventional amplifier employed in a receiver system and the filter direct-coupled amplifier

2 Active *N*+3 coupling matrix synthesis

Prototypes of ladder networks are employed to synthesize the classic passive coupling matrix (Cameron et al., 2007; Cameron, 2011). Here, the passive coupling matrix concept will be extended to active multifunctional devices. A complete amplifier circuit model is constructed using LC resonators and J inverters, as shown in Fig. 2a. The load of the filter is replaced by the transistor that has a complex input port (Y_{P_1} is the input port admittance). The transistor is cascaded directly to the resonator via J_Y. Transistor modeling is a mature subject and has yielded highly accurate closed-form equivalent circuits which replicate the measured devices up to millimeter-wave

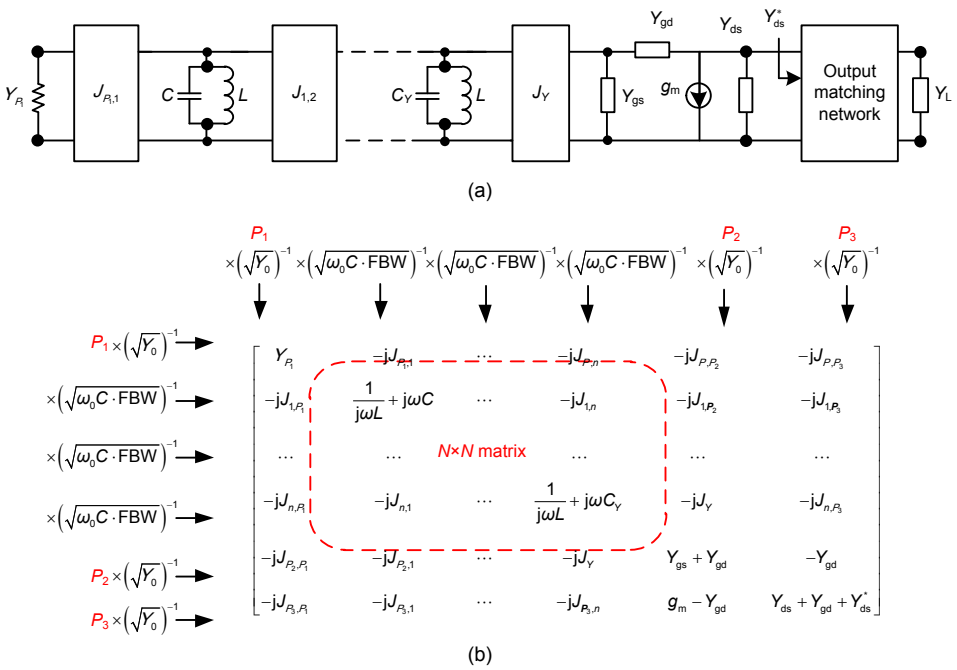

Fig. 2 Simplified lumped circuit of the filter direct-coupled amplifier (a) and matrix [*Y*] of the lumped circuit and matrix scaling operation from [*Y*] to $[\bar{Y}]$ (b)

frequencies (Pozar, 2012). Y_{gs}, Y_{gd}, and Y_{ds} are the admittances, and g_m is the transconductance. Y_{ds} is matched to the load Y_L through the matching network. Y_L is a 50-Ω load. Kirchhoff's laws can be applied to write down the current in each of the resonator loops, resulting in the matrix [*Y*], as shown in Fig. 2b.

The S-parameter responses can be calculated as (Kurokawa, 1965)

$$\begin{cases} S_{11}=2\left|\mathrm{Re}\left(Y_{P_1}\right)\right|[Y]^{-1}_{P_1,P_1}-1, \\ S_{21}=2\sqrt{\left|\mathrm{Re}\left(Y_{P_1}\right)\right|\left|\mathrm{Re}\left(Y_{P_3}\right)\right|}[Y]^{-1}_{P_3,P_1}. \end{cases} \tag{1}$$

The matrix manipulation process is illustrated in Fig. 2b, in which P_1 and P_2 indicate the input and output ports of the filter, respectively, and P_3 represents the output port of the transistor. The elements of the i^{th} row and the j^{th} column (i, j=1, 2, …, n) of matrix [*Y*] are divided by $\sqrt{\omega_0 C\cdot \mathrm{FBW}}$, where $\omega_0=1/\sqrt{LC}$ is the angular center frequency and FBW is the fractional bandwidth. P_1, P_2, and P_3 are divided by $\sqrt{Y_0}$.

Note that the inverses of [*Y*] and $[\bar{Y}]$ can be expressed as (Strang, 2016)

$$\begin{cases} [Y]^{-1}_{P_i,P_j}=\mathbf{cof}\left(Y_{P_i,P_j}\right)\Big/|Y|, \quad |Y|\neq 0, \\ [\bar{Y}]^{-1}_{P_i,P_j}=\mathbf{cof}\left(\bar{Y}_{P_i,P_j}\right)\Big/|\bar{Y}|, \quad |\bar{Y}|\neq 0, \end{cases} \tag{2}$$

where $|Y|$ and $|\bar{Y}|$ are the determinants of [*Y*] and $[\bar{Y}]$, respectively, and $\mathbf{cof}\left(Y_{P_i,P_j}\right)$ and $\mathbf{cof}\left(\bar{Y}_{P_i,P_j}\right)$ are the entries in the i^{th} column and the j^{th} row of the cofactor matrices of [*Y*] and $[\bar{Y}]$, respectively. According to the relationship of matrices [*Y*] and $[\bar{Y}]$, relationships of determinants and cofactors can be expressed as

$$\begin{cases} |Y|^{-1}_{P_i,P_j}=\left(\sqrt{\omega_0 C\cdot \mathrm{FBW}}\right)^{2n}\cdot\left(\sqrt{Y_0}\right)^{6}|\bar{Y}|, \\ \mathbf{cof}\left(Y_{P_i,P_j}\right)=\left(\sqrt{\omega_0 C\cdot \mathrm{FBW}}\right)^{2n}\cdot\left(\sqrt{Y_0}\right)^{4}\mathbf{cof}\left(\bar{Y}_{P_i,P_j}\right). \end{cases} \tag{3}$$

Substituting Eq. (3) into Eq. (2) yields

$$[Y]^{-1}_{P_i,P_j}=\frac{[\bar{Y}]^{-1}_{P_i,P_j}}{Y_0}. \tag{4}$$

Substituting Eq. (4) into Eq. (1) yields

$$\begin{cases} S_{11}=2\left|\mathrm{Re}\left(\overline{Y}_{P_1}\right)\right|[\overline{Y}]^{-1}_{P_1,P_1}-1, \\ S_{21}=2\sqrt{\left|\mathrm{Re}\left(\overline{Y}_{P_1}\right)\right|\left|\mathrm{Re}\left(\overline{Y}_{P_3}\right)\right|}[\overline{Y}]^{-1}_{P_3,P_1}. \end{cases} \tag{5}$$

Applying narrow-band approximation, $[Y]$ can be approximately equal to matrix $[A]$. Given that port admittances $\overline{Y}_{P_1}$ and $\overline{Y}_{P_2}$ are unity, the S-parameters can be calculated as

$$\begin{cases} S_{11}=2[A]^{-1}_{P_1,P_1}-1, \\ S_{21}=2[A]^{-1}_{P_3,P_1}. \end{cases} \tag{6}$$

The active coupling matrix is shown in Fig. 2. The conventional $N\times N$ coupling matrix is surrounded by the additional columns and rows denoting the transistor parameters. Matrix $[A]$ can be expressed as

$$[A]=[T]+p[U]-\mathrm{j}[m]. \tag{7}$$

In Eq. (7), $[T]$ is an admittance matrix, given by

$$[T]=\begin{bmatrix} 0 & 0 & \cdots & 0 & 0 \\ 0 & 0 & \cdots & 0 & 0 \\ \vdots & \vdots & & \vdots & \vdots \\ 0 & 0 & \cdots & \overline{Y}_{\mathrm{gs}}+\overline{Y}_{\mathrm{gd}} & 0 \\ 0 & 0 & \cdots & 0 & \overline{Y}_{\mathrm{gd}}+\overline{Y}_{\mathrm{ds}}+\overline{Y}^{*}_{\mathrm{ds}} \end{bmatrix}. \tag{8}$$

$[U]$ is a diagonal identity matrix. p is given by

$$p=\mathrm{j}\frac{1}{\mathrm{FBW}}\left(\frac{\omega}{\omega_0}-\frac{\omega_0}{\omega}\right). \tag{9}$$

$[m]$ is a coupling matrix. In $[m]$, $m_{i,j}$ is the internal coupling, and $m_{P_{k,i}}$ (k=1, 2, …, n) are the external couplings. m_{P_2,P_3} and m_{P_3,P_2} are the couplings in the active device, given by

$$m_{P_2,P_3}=\frac{\overline{Y}_{\mathrm{gd}}}{\mathrm{j}},\ m_{P_3,P_2}=\frac{\overline{Y}_{\mathrm{gd}}-\overline{g}_{\mathrm{m}}}{\mathrm{j}}. \tag{10}$$

The coupling coefficients are modified by

$$m_{n,n}=-\frac{b}{ag_ng_{n+1}}, \tag{11}$$

$$m_{n,P_2}=m_{P_2,n}=\sqrt{\frac{a^2+b^2}{ag_ng_{n+1}}}, \tag{12}$$

where g_n and g_{n+1} are the standard g-values in the filter design. a and b are the normalized real and imaginary parts of $\overline{Y}_{\mathrm{in}}$, given by

$$a=\mathrm{Re}\left(\frac{\overline{Y}_{\mathrm{gd}}[\overline{g}_m+\overline{Y}_{\mathrm{ds}}+\overline{Y}^{*}_{\mathrm{ds}}]}{\overline{Y}_{\mathrm{gd}}+\overline{Y}_{\mathrm{ds}}+\overline{Y}^{*}_{\mathrm{ds}}}+\overline{Y}_{\mathrm{gs}}\right), \tag{13}$$

$$b=\mathrm{Im}\left(\frac{\overline{Y}_{\mathrm{gd}}[\overline{g}_m+\overline{Y}_{\mathrm{ds}}+\overline{Y}^{*}_{\mathrm{ds}}]}{\overline{Y}_{\mathrm{gd}}+\overline{Y}_{\mathrm{ds}}+\overline{Y}^{*}_{\mathrm{ds}}}+\overline{Y}_{\mathrm{gs}}\right), \tag{14}$$

$$\overline{Y}_{\mathrm{in}}=a+\mathrm{j}b.$$

The response of the multifunctional circuit in Fig. 2a can be calculated by Eq. (6). Through the matrix scaling process, the coupling matrix in Fig. 2b enables the filtering responses (Chebyshev, Butterworth, ellipse, and etc.) to be maintained.

After the active matrix is synthesized, it is used in the design of the filter amplifier. Fig. 3 shows the topology of the filter direct-coupled amplifier and the corresponding equivalent lumped circuits.

The internal couplings $M_{i,j}$ are calculated as the conventional filter synthesis:

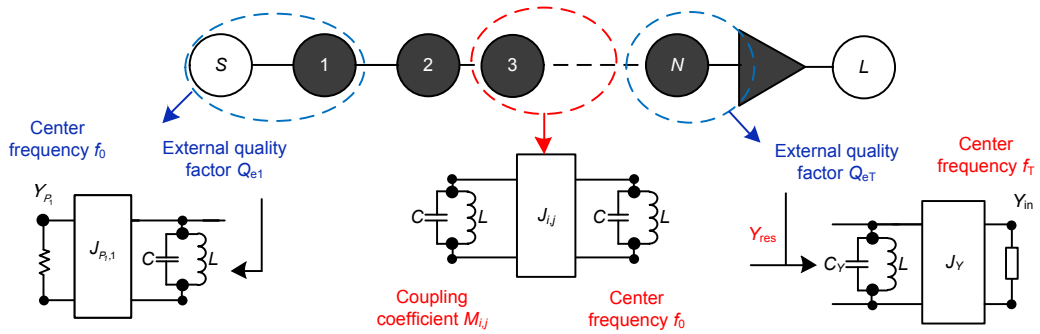

Fig. 3 Topology of the filter direct-coupled amplifier and the corresponding circuits

$$M_{i,j}=\mathrm{FBW}\cdot m_{i,j},\quad i,j=1,2,...,n. \tag{15}$$

The external coupling Q_{e1} is calculated by

$$Q_{e1}=\frac{1}{\mathrm{FBW}\cdot m_{1,P_1}^2}=\frac{1}{\mathrm{FBW}\cdot m_{P_1,1}^2}. \tag{16}$$

From Eq. (16) the required Q_{e1} can be found. As illustrated in Fig. 3, the equivalent input admittance Y_{in} is calculated by

$$Y_{in}=(a+\mathrm{j}b)Y_0. \tag{17}$$

The self-coupling $m_{n,n}$ depends on the center resonance frequency, and the external couplings $m_{P_2,n}=m_{n,P_2}$ depend on the coupling strength to the transistor. In a filter direct-coupled amplifier device, external couplings $m_{P_2,n}=m_{n,P_2}$ and the self-coupling $m_{n,n}$ are related to the center frequency f_T and the external quality factor Q_{eT}. As shown in Fig. 3, this resonator includes Y_{in}, the N^{th} resonator, and the inverter J_Y. Since $m_{n,n}$, m_{n,P_2}, and $m_{P_2,n}$, are given in Eqs. (11) and (12), frequency f_T and Q_{eT} can be calculated by

$$f_T=f_0, \tag{18}$$

$$Q_{eT}=\frac{q_{en}}{\mathrm{FBW}}, \tag{19}$$

where f_0 is the center frequency and q_{en} is the normalized quality factor of the N^{th} resonator. According to Eq. (19), in our case, Q_{eT} is equal to the external quality factor of resonator Q_{e2}.

3 The X-band microstrip filter amplifier

After the active coupling matrix has been synthesized, a microstrip filter direct-coupled amplifier is designed. We use a pair of hairpin resonators to form the filter, as shown in Fig. 4, which also gives the illustrated layout. The second-order hairpin filter is constructed in the input of the transistor as the filter matching network. The second resonator is directly coupled to the transistor footprint. A single stub acts as the output matching. The geometries of the filter are determined by the coupling matrix synthesized above and the extraction procedure will be discussed.

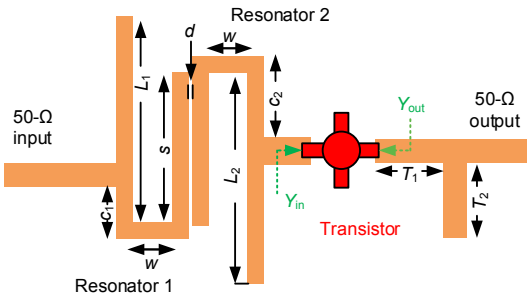

Fig. 4 Layout of the microstrip filter direct-coupled amplifier

The center frequency of the hairpin resonator is determined by multiple parameters, s, w, L_1, and L_2. The tapping distance c_1 determines the external coupling strength to resonator 1. The same mechanism applies to resonator 2, where the tapping distance c_2 affects the quality factor Q_{eT}. The active circuit design approach employed here resembles the classic passive filter design synthesis, and the physical construction design procedure will be described below.

Matrix $[m]$ is calculated according to the prescribed filter specifications. As shown in Fig. 4, a two-pole filter (N=2) is proposed as an example. The center frequency f_0 is designed as 10 GHz, with a bandwidth of 500 MHz (FBW=0.05) and a return loss of 20 dB over the passband. We use the NE310S01 transistor (NE310S01, California, USA) as the active device, and its parameters of the normalized matrix $[Y]$ can be found.

According to the filter specifications and Eqs. (9)–(12), $[m]$ can be calculated and is given in Eq. (20) at the bottom of this page.

Matrix $[T]$ is calculated as

$$[m]=\begin{bmatrix} 0 & 1.2264 & 0 & 0 & 0 \\ 1.2264 & 0 & 1.6621 & 0 & 0 \\ 0 & 1.6621 & -1.0762 & 2.3407 & 0 \\ 0 & 0 & 2.3407 & 0 & 0.1629-0.0164\mathrm{j} \\ 0 & 0 & 0 & 6.9129+3.465\,78\mathrm{j} & 0 \end{bmatrix}. \tag{20}$$

$$[T]=\begin{bmatrix}1&0&0&0&0\\0&0&0&0&0\\0&0&0&0&0\\0&0&0&0.2692+1.5428\mathrm{j}&0\\0&0&0&0&0.5668+0.1630\mathrm{j}\end{bmatrix}. \tag{21}$$

Using Eqs. (6) and (20), matrix $[A]$ can produce the S-parameter response, as shown in Fig. 5, which shows a standard Chebyshev filter response and a gain.

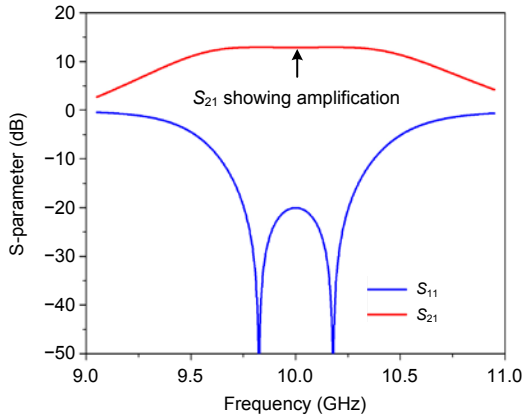

Fig. 5 Active matrix calculated S-parameter response of filter direct-coupled amplifier (References to color refer to the online version of this figure)

Referring to Eq. (16), the external quality factor Q_{e1} is calculated as 13.297. Inter-resonator coupling $M_{1,2}$ is 0.0831 according to Eq. (20). Applying Eqs. (18)–(20), Q_{eT} and f_T are calculated as 13.297 and 10 GHz, respectively. Next, the physical dimensions will be determined from these coupling coefficients and the external quality factor. A single hairpin resonator is constructed and simulated in the Keysight advanced design system (ADS), as shown in Fig. 6a. A single resonance response is simulated to facilitate the extraction of the Q factor. All parameters are set to be constant except for c_1 and L_1. By adjusting c_1, the relationship between the physical parameter and Q can be established as shown in Fig. 6b. During the design process, s and w are 3.15 and 1 mm, respectively. L_1 is tuned to ensure that the resonant frequency remains at 10 GHz when c_1 varies.

Two coupled microstrip hairpin resonators are configured to extract the internal coupling coefficient, as shown in Fig. 7a. The width of the resonator is identical to that of the single resonator discussed above. Different from the single resonance curve, the coupling responses with two resonant peaks are obtained in the ADS. The distance of the peaks of the coupling curve is determined by the width of the gap d. The hairpin arm length L is tuned to compensate for the center frequency shift. The relationship between d and $M_{1,2}$ is illustrated in Fig. 7b, and the required width of d (to provide the desired coupling coefficients) can be acquired from the curve. During the design process, the other dimension values L, s, and w keep constant and are 4, 3.15, and 1 mm, respectively.

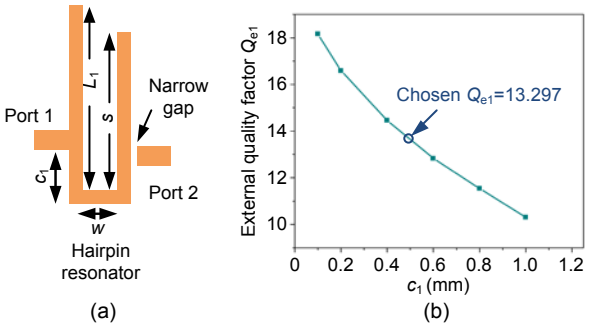

Fig. 6 Extraction of Q_{e1}: (a) single microstrip hairpin resonator to extract Q_{e1}; (b) relationship of Q_{e1} and c_1

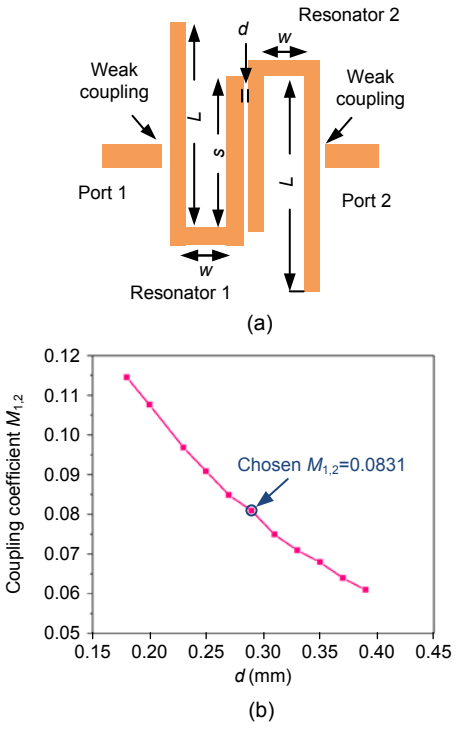

Fig. 7 Coupled hairpin resonators for $M_{1,2}$ extraction (a) and relationship of $M_{1,2}$ and d (b)

The extraction of Q_{eT} is a different procedure because the whole structure includes the resonator itself and the load Y_{in}. Compared to the single resonator, the load Y_{in} is coupled to the microstrip, as shown Fig. 8a. The adhered transistor affects the center frequency, and this frequency shift can be compensated for by adjusting L_2. This center frequency change corresponds to the self-coupling $M_{2,2}$. The relationship between Q_{e2} and c_2 is depicted in Fig. 8b.

As the last step, the output matching of the microstrip transistor circuit is designed. As illustrated in Fig. 2, the output drain to source admittance of transistor Y_{ds} is proposed to use the conjugate matching technique. The single stub with 50-Ω character impedance can be used as a matching network because of its simple structure and ease to manufacture. Classic Smith chart matching technique is employed to determine the values of T_1 and T_2 (Pozar, 2012). The bias circuit is designed using the quarter transmission line method to provide an open-end effect at 10 GHz (the center frequency). Soldering pads are included at the end of the bias tees to offer direct current (DC) power. The simulated operating conditions are given by V_{ds}=2 V and I_{ds}=10 mA. The layout of the microstrip filter direct-coupled amplifier is presented in Fig. 9. The through-holes provide two pins of the source.

After the initial physical dimensions have been extracted, the amplifier is optimized in the ADS. Fig. 10 shows the simulation results before and after optimization. The solid curves in Figs. 10a and 10b are the optimized S-parameter responses, and the dashed lines are the responses of the initial values.

The reflection poles become evident after optimization. The reflection poles of the Chebyshev filtering response can be clearly seen from S_{11}. S_{21} exhibits a gain of 12 dB across the range from 9.75 to 10.25 GHz. The optimized parameters are compared with the initial values in Table 1. For completeness, the stability factors simulated as shown in Fig. 10c indicate the unconditional stable state from DC to 20 GHz. The simulated noise figure is presented in Fig. 10d, with a minimum value of 1.01 dB achieved at 9.88 GHz.

4 Fabrication and measurement

The microstrip filter amplifier was manufactured using a printed circuit process. The Rogers RT/5870,

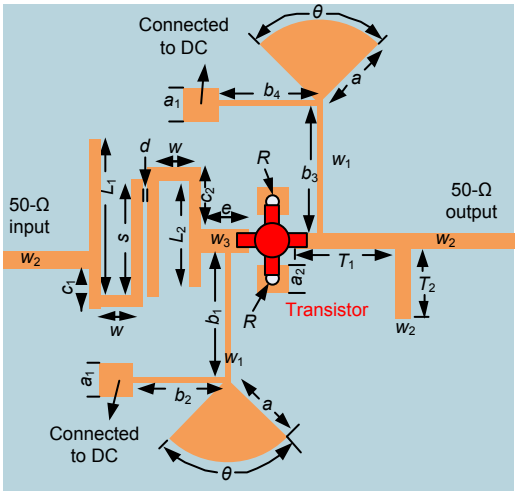

Fig. 9 Layout of the microstrip filter direct-coupled amplifier

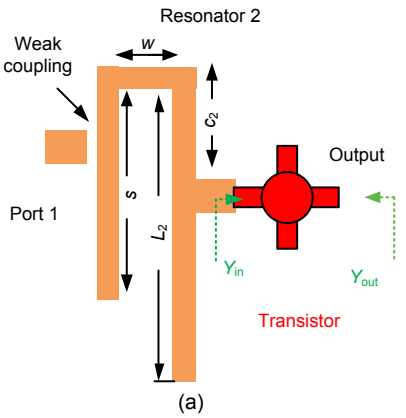

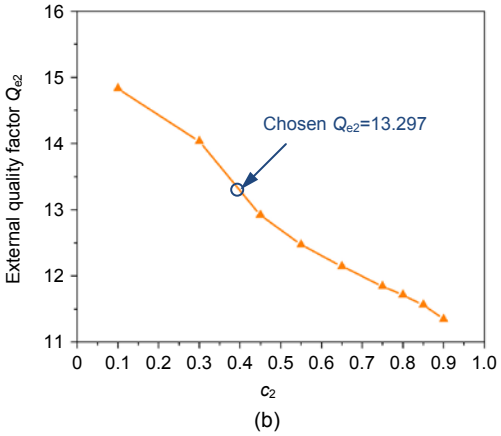

Fig. 8 Configuration of extracting Q_{e2}: (a) layout of the hairpin resonator coupled to the transistor; (b) relationship of Q_{e2} and c_2

Table 1 Values of the initial and optimized microstrip filter direct-coupled parameters

Parameter	Initial	Optimized	Parameter	Initial	Optimized	Parameter	Initial	Optimized
L_1 (mm)	4.10	4.14	θ (°)	70	70	a_1 (mm)	1.20	1.20
L_2 (mm)	3.88	3.71	b_1 (mm)	6.50	6.32	T_1 (mm)	3.80	3.66
c_1 (mm)	0.43	0.81	b_2 (mm)	2.20	2.20	T_2 (mm)	3.10	2.25
c_2 (mm)	0.38	1.30	b_3 (mm)	5.50	4.95	w (mm)	1.00	1.00
s (mm)	3.15	3.07	b_4 (mm)	2.20	2.20	w_1 (mm)	0.30	0.30
d (mm)	0.25	0.15	a (mm)	3.32	3.32	w_2 (mm)	0.78	0.78
R (mm)	0.50	0.50	e (mm)	1.10	1.16	w_3 (mm)	1.20	1.67

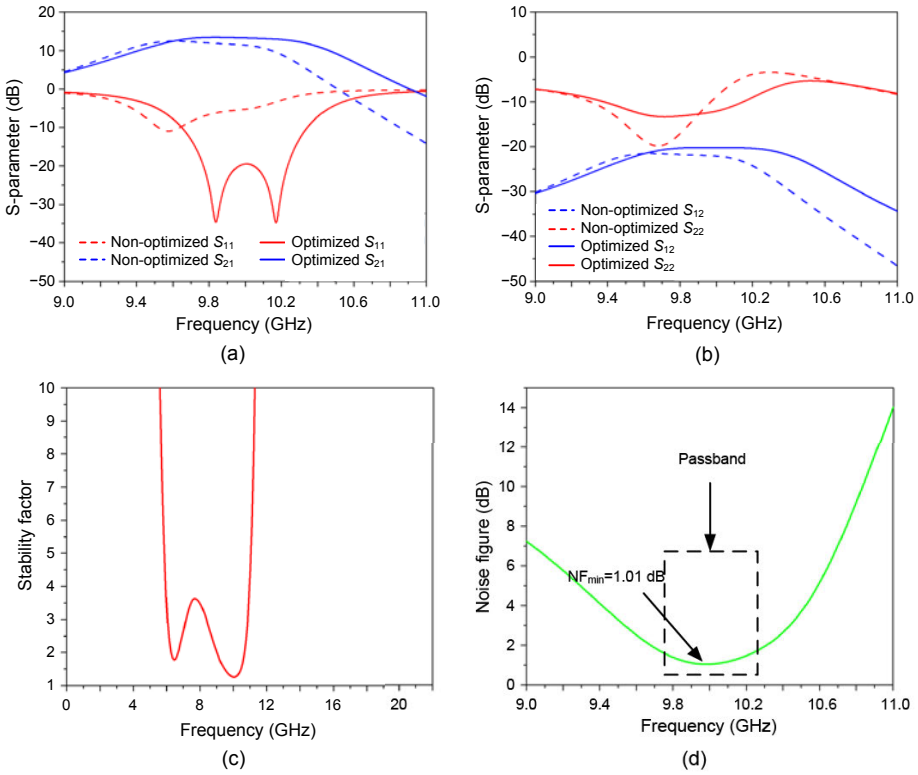

Fig. 10 Simulated response of the amplifier before and after optimization: (a) S_{11} and S_{21}; (b) S_{22} and S_{12}; (c) stability factor; (d) noise figure

with a thickness of 0.254 mm and a relative dielectric constant of 2.33, was used as the substrate. The photograph of the fabricated device is shown in Fig. 11. A Keysight E8362B PNA network analyzer (E8362B, California, USA) was employed to measure the device.

Fig. 12 gives the measurement results of the filter amplifier. The solid lines correspond to the measurement results and the dashed lines stand for the simulation results. 10-dB gain is achieved over the passband for the amplifier. The maximum return loss across the passband at the input port is measured to be around −8 dB, as shown in Fig. 12a. The output port also achieves a good match, as shown in Fig. 12b.

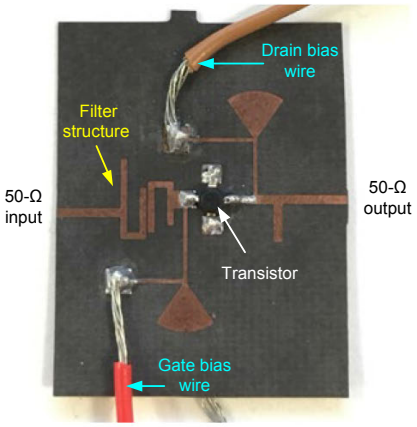

Fig. 11 Photograph of the X-band microstrip filter amplifier

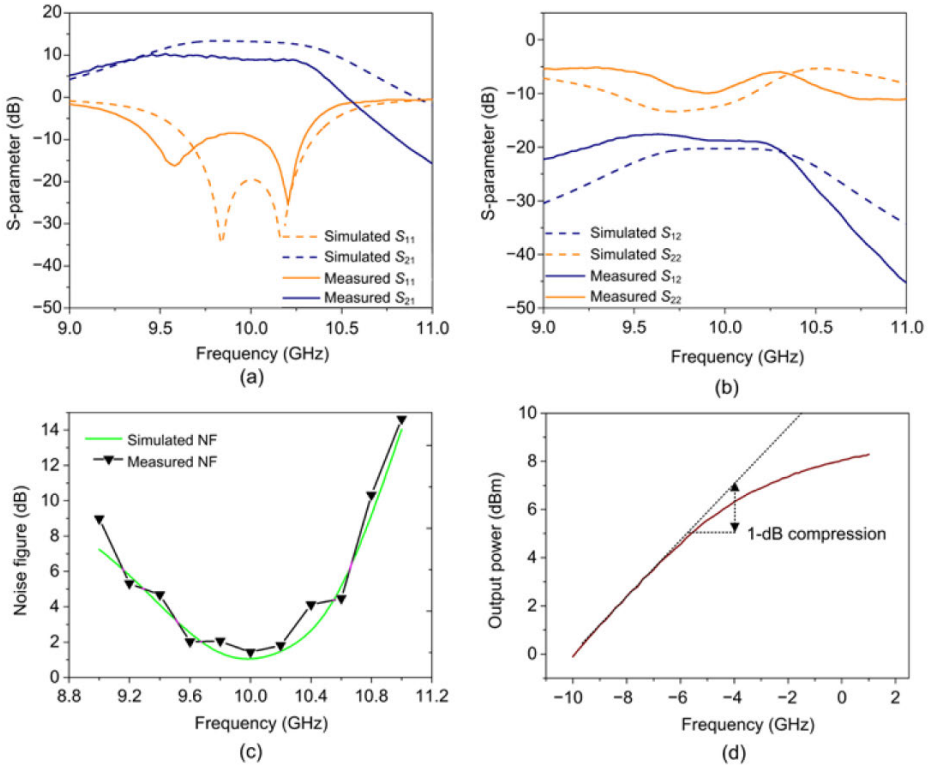

Fig. 12 Measurement and simulation results: (a) S_{11} and S_{21}; (b) S_{22} and S_{12}; (c) noise figure; (d) P1-dB measurement

Fig. 12c shows the measured and simulated noise figures of the integrated device. The 1-dB compression (P1-dB) measurement results are presented in Fig. 12d. Generally, the measurement results agree well with the simulation results, verifying the effectiveness of the filter amplifier design approach. The differences between the simulation and measurement results are believed to be attributed to fabrication errors.

5 Conclusions

In this paper, an active coupling matrix representing a filter direct-coupled amplifier has been synthesized. Matrix manipulation and a scaling process have been performed to construct this novel active coupling matrix. An X-band microstrip filter amplifier with Chebyshev filtering response has been designed as an example. The active coupling matrix, extended from the classical matrix for filters, has been derived to include active devices, e.g., amplifiers. The matrix can be adopted for other types of devices with complex ports, e.g., mixers and frequency multipliers.

Contributors

Yang GAO and Lei LI designed the research. Fan ZHANG and Jiawei ZANG manufactured and measured the device. Yang GAO drafted the manuscript. Lei LI, Yingying QIAO, and Xiaobang SHANG revised and finalized the paper.

Compliance with ethics guidelines

Yang GAO, Fan ZHANG, Yingying Qiao, Jiawei ZANG, Lei LI, and Xiaobang SHANG declare that they have no conflict of interest.

References

Aljarosha A, Zaman AU, Maaskant R, 2017. A wideband contactless and bondwire-free MMIC to waveguide transition. *IEEE Microw Wirel Compon Lett*, 27(5):437-439. https://doi.org/10.1109/LMWC.2017.2690846

Bahl IJ, 2008. Fundamentals of RF and Microwave Transistor Amplifiers. Wiley, Hoboken, USA. https://doi.org/10.1002/9780470462348

Cameron RJ, 2011. Advanced filter synthesis. *IEEE Microw Mag*, 12(6):42-61. https://doi.org/10.1109/MMM.2011.942007

Cameron RJ, Kudsia CM, Mansour RR, 2007. Microwave Filters for Communication Systems: Fundamentals, Design and Applications. Wiley, Hoboken, USA.

Chang CY, Itoh T, 1990. Microwave active filters based on coupled negative resistance method. *IEEE Trans Microw Theory Tech*, 38(12):1879-1884.

https://doi.org/10.1109/22.64569

Chen KL, Lee J, Chappell WC, et al., 2013a. Co-design of highly efficient power amplifier and high-*Q* output bandpass filter. *IEEE Trans Microw Theory Tech*, 61(11): 3940-3950. https://doi.org/10.1109/TMTT.2013.2284485

Chen KL, Lee TC, Peroulis D, 2013b. Co-design of multi-band high-efficiency power amplifier and three-pole high-*Q* tunable filter. *IEEE Microw Wirel Compon Lett*, 23(12): 647-649. https://doi.org/10.1109/LMWC.2013.2283876

Chun YH, Yun SW, Rhee JK, 2002. Active impedance inverter: analysis and its application to the bandpass filter design. Proc IEEE MTT-S Int Microwave Symp, p.1911-1914. https://doi.org/10.1109/MWSYM.2002.1012237

Chun YH, Lee JR, Yun SW, et al., 2005. Design of an RF low-noise bandpass filter using active capacitance circuit. *IEEE Trans Microw Theory Tech*, 53(2):687-695. https://doi.org/10.1109/TMTT.2004.840565

Courtney PG, Zeng J, Tran T, et al., 2015. 120W Ka band power amplifier utilizing GaN MMICs and coaxial waveguide spatial power combining. Proc IEEE Compound Semiconductor Integrated Circuit Symp, p.1-4. https://doi.org/10.1109/CSICS.2015.7314457

Darcel L, Dueme P, Funck R, et al., 2005. New MMIC approach for low noise high order active filters. Proc IEEE MTT-S Int Microwave Symp, p.787-790. https://doi.org/10.1109/MWSYM.2005.1516731

Gao Y, Powell J, Shang XB, et al., 2018. Coupling matrix-based design of waveguide filter amplifiers. *IEEE Trans Microw Theory Tech*, 66(12):5300-5309. https://doi.org/10.1109/TMTT.2018.2871122

Gao Y, Shang XB, Guo C, et al., 2019. Integrated waveguide filter amplifier using the coupling matrix technique. *IEEE Microw Wirel Compon Lett*, 29(4):267-269. https://doi.org/10.1109/LMWC.2019.2901892

Gao Y, Zhang F, Lv X, et al., 2020. Substrate integrated waveguide filter–amplifier design using active coupling matrix technique. *IEEE Trans Microw Theory Tech*, 68(5):1706-1716. https://doi.org/10.1109/TMTT.2020.2972390

Gonzalez G, 1996. Microwave Transistor Amplifiers: Analysis and Design (2nd Ed.). Prentice Hall, Pearson, UK.

Ito M, Maruhashi K, Kishimoto S, et al., 2004. 60-GHz-band coplanar MMIC active filters. *IEEE Trans Microw Theory Tech*, 52(3):743-750. https://doi.org/10.1109/TMTT.2004.823531

Kumar TB, Ma KX, Yeo KS, 2017. A 60-GHz coplanar waveguide-based bidirectional LNA in SiGe BiCMOS. *IEEE Microw Wirel Compon Lett*, 27(8):742-744. https://doi.org/10.1109/LMWC.2017.2723951

Kurokawa K, 1965. Power waves and the scattering matrix. *IEEE Trans Microw Theory Tech*, 13(2):194-202. https://doi.org/10.1109/TMTT.1965.1125964

Lin YS, Wu JF, Hsia WF, et al., 2013. Design of electronically switchable single-to-balanced bandpass low-noise amplifier. *IET Microw Antenn Propag*, 7(7):510-517. https://doi.org/10.1049/iet-map.2012.0426

Pozar DM, 2012. Microwave Engineering (4th Ed.). Wiley, New York, USA.

Schwierz F, Liou JJ, 2002. Modern Microwave Transistors: Theory, Design, and Performance. Wiley, Hoboken, USA.

Strang G, 2016. Introduction to Linear Algebra (5th Ed.). Wellesley-Cambridge Press, Wellesley, USA.